Actuatable Membranes Based on Polypyrrole-Coated Vertically Aligned Carbon Nanofibers

Benjamin L. Fletcher,[†,‡] Scott T. Retterer,[†,§,∥] Timothy E. McKnight,[†,⊥] Anatoli V. Melechko,[†,∥] Jason D. Fowlkes,[†,‡] Michael L. Simpson,[†,‡,∥] and Mitchel J. Doktycz[†,§,∥,*]

[†]Molecular Scale Engineering and Nanoscale Technologies Research Group, Materials Science and Technology Division, Oak Ridge National Laboratory, Bethel Valley Road, Oak Ridge, Tennessee 37831, [‡]Materials Science and Engineering Department, University of Tennessee, 434 Dougherty Hall, Knoxville, Tennessee 37996, [§]Biological and Nanoscale Systems Group, Biosciences Division, Oak Ridge National Laboratory, Oak Ridge, Tennessee 37831, [⊥]Monolithic Systems Group, Engineering Science and Technology Division, Oak Ridge National Laboratory, Oak Ridge, Tennessee 37831, and [∥]Center for Nanophase Materials Sciences, Oak Ridge National Laboratory, Oak Ridge, Tennessee 37831

ABSTRACT Nanoporous membranes are applicable to a variety of research fields due to their ability to selectively separate molecules with high efficiency. Of particular interest are methods for controlling membrane selectivity through externally applied stimuli and integrating such membrane structures within multiscale systems. Membranes comprised of deterministically grown, vertically aligned carbon nanofibers (VACNFs) are compatible with these needs. VACNF membranes can regulate molecular transport by physically selecting species as they pass between the fibers. Defined interfiber spacing allows for nanoscale control of membrane pore structure and resultant size selectivity. Subsequent physical or chemical modification of VACNF structures enables the tuning of physical pore size and chemical specificity allowing further control of membrane permeability. In this work, the dynamic physical modulation of membrane permeability that results when VACNFs are coated with an electrically actuatable polymer, polypyrrole, is demonstrated. Electrochemical reduction of polypyrrole on the VACNFs results in controlled swelling of the diameter of the nanofibers that in turn decreases the pore size. Dynamic control of membrane pore size enables selective transport and gating of nanoscale pores.

KEYWORDS: carbon nanofibers · polypyrrole · electropolymerization · surface modification · nanomaterial · actuation · membranes · nanopore

The controlled synthesis of nanoporous membranes (defined by pores less than 100 nm in width) is enabling for a variety of applications including separations,[1–3] molecular sensing,[4–7] and drug delivery.[8–10] The ability to selectively mediate molecular transport using nanoscale channels is critical for these applications. Nanoporous membranes offer spatial selectivity and high efficiency.[11] However, a major challenge is the construction and integration of nanoporous membranes within multiscale systems, while retaining the ability to regulate the transport of small particles with precision, selectivity, and control.

One approach to synthesizing nanoporous membranes has been to modify naturally occurring membrane proteins, such as α-hemolysin and the mechanosensitive channel of large conductance (MscL) from *Escherichia coli*, to act as nanoscale gate valves.[12–16] These proteins have been modified to switch between open and closed states in response to specific chemical, electrical, and mechanical stimuli. In applications such as molecular sensing, biological nanopores remain the gold standard by which other nanopores are judged. However, membranes constructed from these biological components can be fragile, be difficult to incorporate within macroscalar systems, and provide only fixed-dimension pores.

Alternatively, synthetic analogues that mimic the gating functionality of biological nanopores are being developed as alternatives. Nanoporous membranes have been synthesized using porous alumina,[17] by track etching of nanopores in polymer films,[20–23] from carbon nanotubes embedded in thin polymer films,[24,25] by ion beam etching of oxide films,[26,27] and using soft lithography.[28] These synthetic membranes are fairly robust when compared to biological structures. They offer adjustable surface properties, control over pore diameter and membrane thickness, and routes for integration within micro- and macroscalar systems and devices.

Another approach to synthesizing nanoporous membranes is by creating obstacles in the path of transport. Such structures can be created by "top-down" micro- and nanofabrication techniques[29–31] and by the deterministic growth of vertically aligned carbon nanofibers (VACNFs).[32–35] VACNFs can be grown with control over nanofiber length, diameter, shape, posi-

*Address correspondence to doktyczmj@ornl.gov.

Received for review September 5, 2007 and accepted December 21, 2007.

Published online January 15, 2008.
10.1021/nn700212k CCC: $40.75

tion, orientation, and chemical composition.[36–38] Within an ensemble of nanofibers that makeup a microscale membrane structure, such control allows for precise engineering of critical dimensions such as interfiber spacing and membrane thickness, which dictate membrane permeability and size selectivity. Furthermore, the catalytic growth of carbon nanofibers allows for nanoscale functionality to emerge from simple microscale lithography techniques. VACNF growth typically yields individual nanofibers up to several hundred nanometers in diameter, spaced several hundred nanometers apart. As a result, membranes of carbon nanofibers, patterned using techniques such as contact photolithography, have nanoscale features that emerge during synthesis.

Interfiber spacing, and resultant membrane pore size, can be further tuned through physical modification or coating of the nanofibers. Modification by oxide deposition or electropolymerization of polypyrrole (pPy) has been demonstrated.[35,39–41] Because VACNFs possess electrochemical properties similar to those found in carbon-based electrodes,[42] conductive polymers such as pPy can be electrochemically synthesized on the active surface areas to controllably modify fiber dimensions and surface energy.[41,43] In addition to passive adjustment of pore size, the physical volume of the pPy coating can be controllably altered by electrical stimuli,[44–51] providing a means to dynamically modulate membrane permeability and size selectivity.

In this work, the synthesis and demonstration of hybrid carbon nanofiber based, actuatable polymer membranes in microfluidic manifolds, representing the first steps toward the creation of devices with electrically controllable, dynamic membrane structures, is described. The actuatable polymer, pPy, was electrochemically deposited on the sidewalls of vertically aligned carbon nanofibers. Altered transport of variously sized fluorescent species was achieved by actuation of the nanoscale pores created by the interfiber spacing. Membrane permeability was modulated by external electrical control. The membranes are relatively thin, as compared to through pores in oxide or polymer films, yet are highly robust. Because of the short transport distances, species can diffuse rapidly through the membrane. In addition, these structures were integrated within devices featuring multiscale components using conventional microfabrication techniques. VACNF membrane structures will enable fundamental studies of biochemical reaction systems and will facilitate the development of new technologies for chemical sampling, biosensing, and pharmaceutical dosing.

RESULTS AND DISCUSSION

Polypyrrole is an electrically conductive, biocompatible polymer whose physical and chemical properties are well-characterized. High-quality, stable films are relatively easy to prepare at low temperatures (25 °C) and under aqueous conditions.[43,44] Oxidation of the monomer results in a polymer film forming on the anode. The polymer coating can be controllably expanded and contracted when the oxidation state of the polymer film is changed in the presence of an electrolyte. The mechanics of this reaction have been extensively described.[45–49] Here, the large anion, dodecylbenzenesulfonate (DBS), is incorporated within the pPy matrix

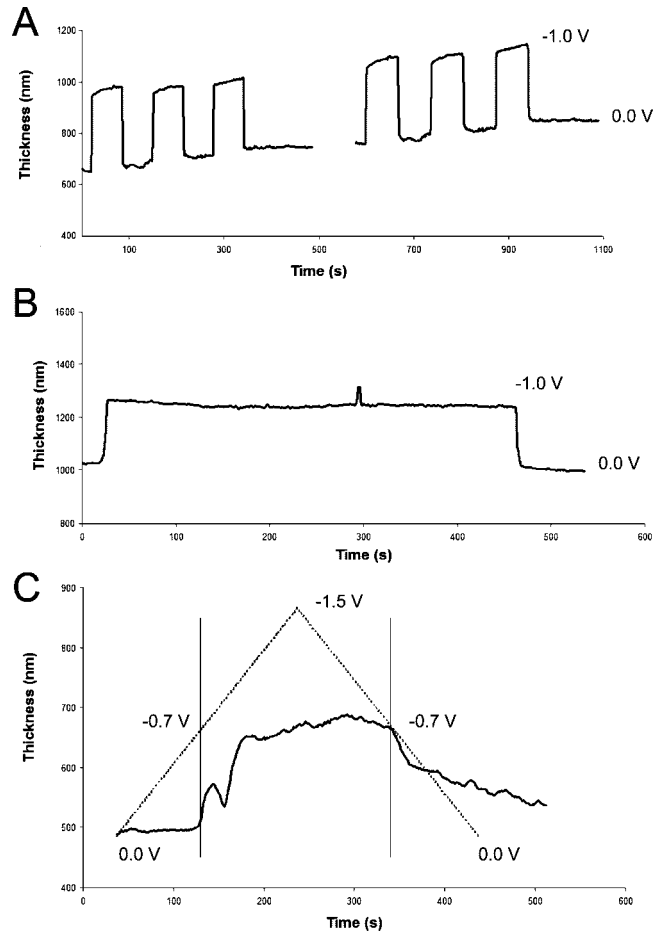

Figure 1. A series of pPy actuations as measured from longitudinal cross sections of a pPy film by performing continuous line scans using an AFM. The pPy film swells when –1.0 V is applied and shrinks when 0.0 V is applied. (A) Repeated actuations, by applying step potentials at –1.0 V for 30 s followed by 0.0 V for 30 s. The discontinuity represents the time elapsed between the two consecutive actuation experiments. (B) An extended actuation, by applying a voltage of –1.0 V for 400 s. (C) pPy actuation as related to applied potential. The solid line represents the measured pPy(DBS) film thickness. The dotted line represents the corresponding applied potential. The vertical lines denote where volume changes in the pPy film begin to occur.

during polymerization to balance the positive charge of the oxidized polymer. The anion is relatively large and becomes trapped during polymerization of the polymer matrix. When the polymer/anion matrix is reduced, cations from the surrounding electrolyte rush in to balance the charge, resulting in an increase in volume and swelling of the polymer.[48,49]

The process of volume expansion/contraction that pPy undergoes has been described previously.[45–49] Additionally, the nanoscale actuation properties of pPy films incorporating dodecylbenzenesulfonate, pPy(DBS), have been characterized by atomic force microscopy (AFM).[50,51] The AFM is used essentially as a highly sensitive profilometer, measuring height differences between the underlying planar electrode and the top of the film. The AFM allows for *in situ* measurement and a high degree of control over the amount of force exerted by the stylus. Therefore, to guide the preparation of pPy-coated CNF membranes, initial studies used gold planar electrodes to evaluate the characteristics of the pPy(DBS) films that would be applied to the CNF-based structures. The maintenance of the volume change under prolonged actuation, the reproducibility of the volume expansion/contraction upon multiple actuations, and the effects of applied potential were examined. Polypyrrole films were then synthesized on the electrically active surface areas of carbon nanofiber membrane structures and evaluated in microfluidic structures. The ability to alter the permeability of the CNF membranes by actuation was evaluated.

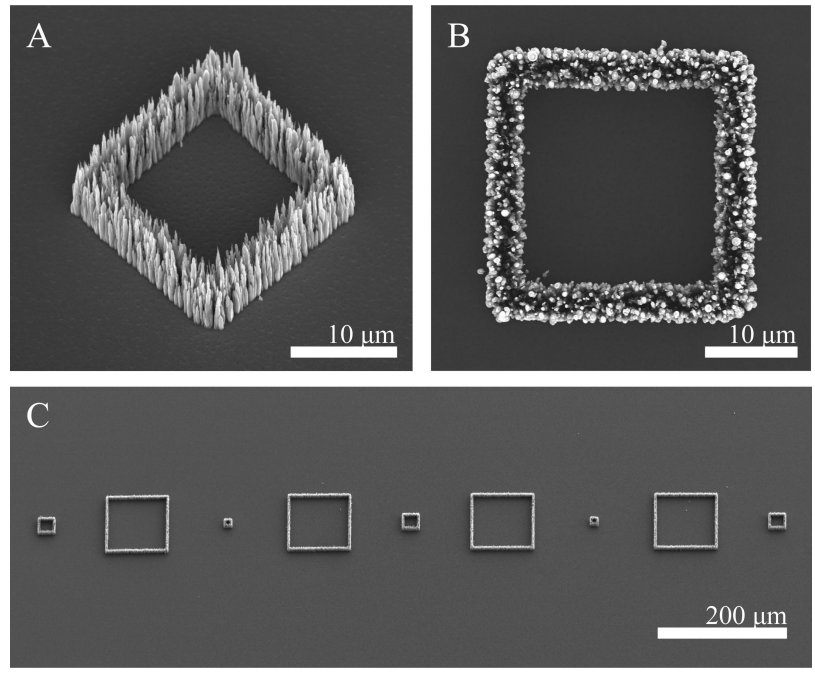

Figure 2. Electron micrographs of the VACNF membrane structures. The membrane structures were grown as 10, 25, 50, 100, and 150 μm square cells with walls 2 μm wide, on a 500 Å Ti substrate. Carbon nanofibers were generally 8.5–9.5 μm tall. Shown in (A) is an electron micrograph of a 25 μm square cell taken at a 30° tilt while (B) is a top view of the same structure and (C) shows a top view of the array of different sized membrane structures.

Planar Electrode Experiments. Actuation experiments on gold planar electrodes were conducted using previously described techniques.[50,51] Swelling and shrinking of the pPy(DBS) films were controlled by applying −1.0 and 0.0 V potentials *versus* a known reference. A series of six actuations was measured by continuous line scans using AFM. Resulting changes in film thickness relative to the underlying gold substrate *versus* time can be seen in Figure 1A. The upward slope of the graph is due to tilt in the AFM stage. Voltages were applied in a sequence of step potentials: −1.0 V for 30 s followed by 0.0 V for 30 s. After the first actuation, the film displayed an irreversible increase in thickness, 17% larger than the original state. This observation is consistent with previously reported pPy actuation results.[51] Subsequent actuations, however, are fully reversible with the reduced (swollen) state 35% thicker than the oxidized (shrunken) state. Analysis of the height traces reveals that the expansion and contraction rate of the polymer film is similar and occurs at a rate of 100 nm/s. In Figure 1B, the pPy(DBS) film was reduced (swollen) for an extended amount of time (400 s). The actuated polymer appears to be stable over this time period, as the volume does not significantly change during the actuation. To evaluate the effect of applied voltage, bias was applied to a pPy(DBS) film as a cyclic voltage from 0.0 to −1.5 V at −0.01 V/s. The resulting actuation was observed under the AFM, and the results are presented in Figure 1C. Volume changes in the pPy(DBS) film do not appear to continuously follow applied bias. Instead, actuation appears to occur at applied voltages close to the reported oxidation potential (−0.7 V) of pPy(DBS) films in 100 mM DBS solutions.[47] Further decreases in applied potential had negligible effects on the swelling of the polymer film.

Carbon Nanofiber—Polypyrrole Membrane Experiments. Carbon nanofiber membrane structures were fabricated on titanium-coated silicon wafers. Catalyst stripes, 2 μm wide, were patterned on the wafers in the shape of squares with sides of 10, 25, 50, 100, and 150 μm. Then, carbon nanofibers were grown in a PECVD process from the nickel catalyst stripes to be 8.5–9.5 μm tall with nominal diameters of 500 nm, measured at the base, and 300 nm, measured at the tip. Figure 2 presents scanning electron micrographs of the resulting VACNF membrane structures.

Polypyrrole films were deposited on the surface of carbon nanofiber membrane structures. The deposited films were found to be 150–200 nm, reducing the average interfiber spacing from 600–800 to 250–350 nm (difference of ~45–55%). Films pre-

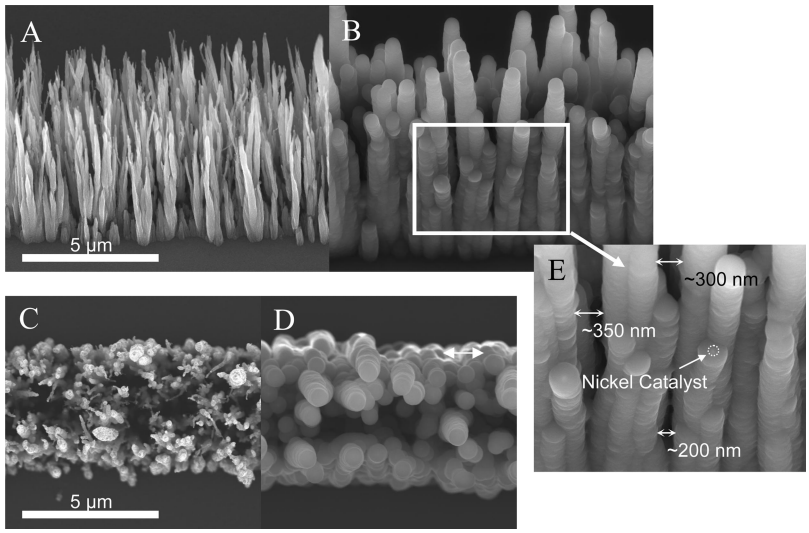

Figure 3. Electron micrographs of a VACNF membrane structure, prior to pPy polymerization (A, C) and after (B, D, E). Polypyrrole films were ~200 nm thick, reducing interfiber spacing from ~600–800 to ~250–350 nm. Thickness measurements were made relative to the diameter of the nickel catalyst (highlighted in E) present at the tip of the nanofiber.

pared on gold planar electrodes in similar reaction conditions were thicker than films prepared on carbon nanofibers. Differences in thicknesses were likely due to the different geometries of the electrodes. After pPy deposition, it was possible to image the underlying nickel catalyst at the tip of the nanofibers using the upper detector of the scanning electron microscope at an acceleration voltage of 10.0 kV. Measurements of resulting pPy film thicknesses were made relative to this feature. Film thickness measurements were confirmed by comparing electron micrographs of the VACNF membranes, before polymerization and after (see Figure 3), using previously described methods.[41]

Swelling and shrinking of the pPy films were controlled by applying −1.0 and 0.0 V potentials. Considering the ~35% volume expansion, the limiting pore size upon actuation should be ~50–250 nm. To test membrane actuation, CNF-based structures were enclosed in simple microfluidic channels and tested with various sized, fluorescently labeled species. Channels were molded in poly(dimethylsiloxane) (PDMS) and were cut with a scalpel to a channel length of ~1.5 mm, long enough to enclose approximately five to seven membrane structures (see Figure 4A). The relatively short channel lengths enabled flow of fluid into the channels during wetting. VACNFs were typically grown to a height of 8.5–9.5 μm while the microfluidic channels were molded to a depth of 5.5 μm. Because of this height differential, the tips of the carbon nanofibers would embed in the PDMS lid after mating.[33] This ensured a good seal between the top of the membrane and the PDMS lid (see Figure 4B).

The VACNF membrane structures were then secured in a Petri dish, along with counter and quasi-reference electrodes. A diagram of the experimental setup can be seen in Figure 4C. During actuation experiments, the pPy on the carbon nanofibers as well as on the titanium substrate would shrink or swell. These shifts in volume of the underlying substrate would cause sealing problems with the PDMS channels. To alleviate this problem, excess pPy was scraped from the titanium substrate with a scalpel prior to mating with the PDMS channels, leaving only a thin (~1 mm) strip of pPy surrounding the VACNF membrane structures. pPy can be observed in Figure 4A as the dark stripe in the middle of the microfluidic channel. The volume change of the remaining pPy on the channel substrate introduced a pumping action to the microfluidic channel. The increased volume of the pPy would displace fluid, pushing fluorescent species out of the channel. Upon shrinking, surrounding fluid and fluorescent species would rush back in. The pumping action facilitated testing of the membrane structures by alleviating the need to integrate other flow control mechanisms. Fluorescent micrographs of an experiment using 321 nm latex beads can be seen in Figure 5. In Figure 5A, the membrane structure is in the "open" state and beads are flowing relatively freely through the structure. The membrane structure shown in Figure 5B was

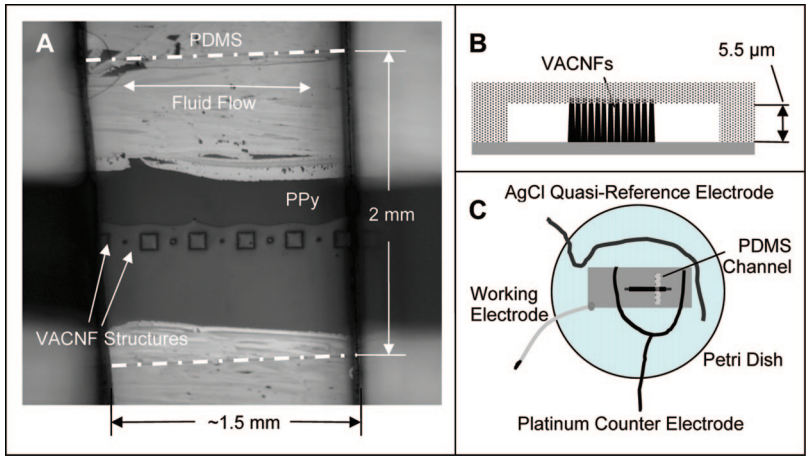

Figure 4. (A) An optical micrograph of the VACNF membrane structure mated with a PDMS microfluidic channel. Channel walls are represented by dotted lines. The PDMS channel is 2 mm wide and ~1.5 mm long. The two structures were aligned and mated by manual manipulation using forceps. Prior to mating, excess pPy was scraped clean from the substrate with a scalpel to improve the seal between the PDMS and the titanium substrate. Remaining pPy appears as the black horizontal stripe. Flow through the channel is from left to right. (B) Graphical representation of the channel interior as viewed down the length of the channel. The microfluidic channel depth was 5.5 μm while nanofibers were grown to heights of 8.5–9.5 μm. (C) Diagrammatic description of the experimental setup (top view) for VACNF membrane structure actuation.

taken 10 s after the pores of the membranes were dilated. Transport is "restricted" and beads are largely excluded from the structure. Flow primarily occurs around the structure. However, fluid flow through the membranes continues as evidenced by the accumulation of beads on the membrane surfaces. The membranes are not completely size selective as some of the trapped beads leak through the structures over time.

The leakiness of the membranes can be attributed to the stochastic arrangement of individual elements within the VACNF forests. The stochastic forests are grown from catalyst nanoparticles formed by dewetting of continuous thin films patterned using contact photolithography. Prior to nanofiber growth the patterned catalyst film is subjected to an ammonia plasma etch at 600 °C. During this etch, the catalyst film breaks up and particles several hundred nanometers in diameter nucleate stochastically at spacings several hundred nanometers apart. While stochastic forests of VACNFs are fabricated using microscalar techniques, they result in nanoscale functionality. However, the stochastic nature of the forests also results in variability in the locations of carbon nanofiber membrane components, affecting interfiber spacings and membrane permeability. Interfiber spacings in portions of the membrane may vary significantly, resulting in regions of relatively higher permeability. This is a phenomenon that may be alleviated by nanoscale lithographic techniques such as electron beam patterning that allows for definition of nanofiber location. Accurate placement of individual membrane components would allow for better control of membrane permeability and membrane actuation properties.

Despite the described limitations, the transport of a wide range of species were modulated by pPy actuation. Changes in permeability through VACNF-based membranes were observed for 200 and 50 nm fluorescently labeled beads, fluorescently labeled streptavidin, and fluorescein isothiocynate (FITC). Fluorescence micrographs showing flow of each of these fluorescent species through similar VACNF-based membrane structures can be seen in Figure 6. The micrographs shown as Figures 6A and 6B were taken ~10 s after flow out of the channel was introduced. In these two experiments, relatively large fluorescent particles were used (200 and 50 nm, respectively). Free flowing fluorescent species have been largely evacuated from the channel while a higher concentration of fluorescent species is found within the VACNF-based membrane structures. The micrographs shown in panels C and D of Figure 6 were taken ~5 s after volume swelling of the pPy was initiated. The particles in these experiments were relatively small. While flow of species through the VACNF membrane structures appears to be more restricted relative to the surrounding free flowing species, the degree of restriction is less for the smaller particles than for the larger latex beads. This is reflected in the brighter background fluorescence in the images.

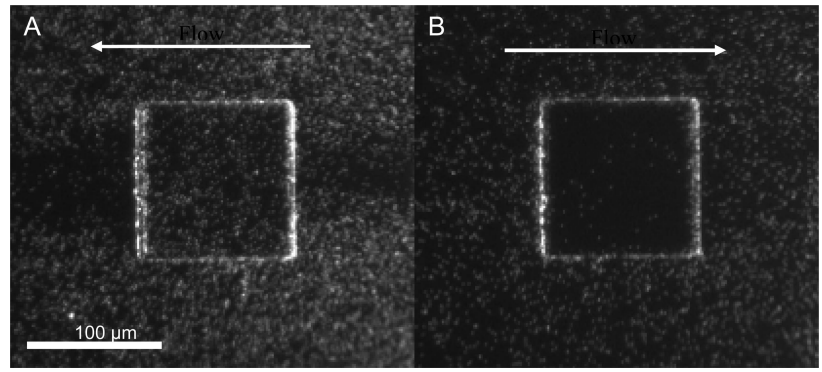

Figure 5. Fluorescent micrographs of 321 nm fluorescently labeled latex beads were taken while beads were flowing through a VACNF membrane structure in (A) "open" and (B) "restricted" transport states. Micrograph B was taken ~10 s after actuation. The interfiber spacing of the VACNF membrane components was decreased by potentiostatically applying −1.0 V to swell the pPy coating and restrict flow. The pores of the membrane were "opened" by removing this bias.

When polypyrrole is actuated, the pores of the VACNF membrane structures are reduced to ~50–250 nm. The pores of the membranes are sufficiently tortuous enough to render the membranes virtually impermeable to the flow of 200 nm beads and restrictive to the flow of smaller species. Larger particles (such as 200 nm beads) collect on the outer membrane walls (see Figure 6A) while smaller particles pass through with little to no noticeable buildup (see Figure 6B−D). However, fluorescent species preferentially flow around the membrane structures where flow is less restrictive, rather than through the membranes. The VACNF membranes are more restrictive to flow when actuated and, as a result, are able to affect the transport of much smaller species (as small as FITC).

The VACNF-based membrane structures could be actuated ~5 times, on average, before failing. The most common source of failure was due to fluidic leaks occurring under the PDMS microfluidic channel. The bond between the PDMS microfluidic channel and the substrate was relatively weak and deteriorated as pressure from fluidic flow was exerted on it. One possible solution would be to incorporate working, counter, and reference electrodes within a microfluidic channel and to seal this channel by clamping. Covalent bonding of the PDMS may also enhance sealing.[52] Despite the described shortcomings, VACNF membrane structures show promise in applications where it is desirable to have membranes that modulate membrane permeability by external electrical control. This can be advantageous for applications that require sampling of a flow stream or controlled dosing of materials. The square-shaped design of the current structures is suitable for these applications and for forming small volume reac-

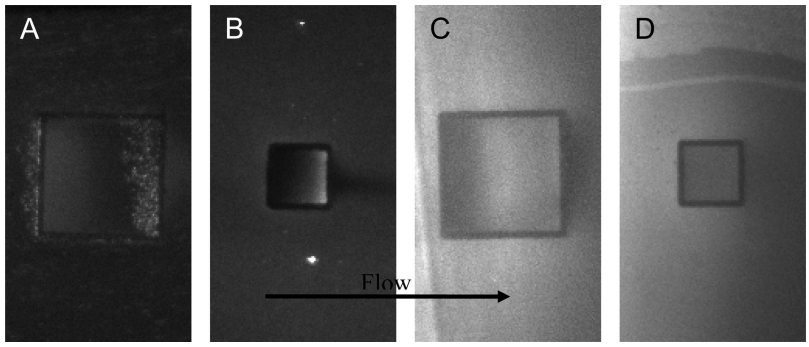

Figure 6. Fluorescent micrographs of (A) 200 nm and (B) 50 nm fluorescently labeled latex beads, (C) fluorescently labeled streptavidin, and (D) FITC were taken while species were flowing through a VACNF membrane structure in the "restricted" flow state. The VACNF membrane structures in (A) and (C) were 150 μm squares and those in (B) and (D) were 50 μm squares.

tion containers of controlled permeability.[33] The described membranes can be made relatively thin, yet robust. This feature allows for short transport distances and higher permeability. Further, the described fabrication process allows for ready integration of micro- and nanoscale elements, facilitating the assembly of multiscalar devices for various uses.

CONCLUSIONS

Carbon nanofiber, actuatable polymer hybrid membranes represent the first steps toward the creation of dynamic membrane structures, capable of reversibly controlling transport on the molecular scale. We describe the fabrication and characterization of these synthetic, actuatable membranes. While vertically aligned carbon nanofibers were patterned using techniques such as contact photolithography, nanoscale features emerged during synthesis. These structures were then integrated within devices featuring multiscale components using conventional microfabrication techniques. Examination of pPy by AFM reveals that pPy volume change is stable for prolonged periods (400 s) and reproducible over multiple actuations. Coating VACNF membrane components with pPy enables modulation of membrane permeability by physically reducing the interfiber spacing and the resultant pore size. Dynamic switching between open and restricted flow states is facilitated by external electrical control. Application of −1.0 V bias to the underlying CNF electrode leads to swelling of the pPy coating and reduced permeability of the membrane. Removal of the bias restores membrane permeability. Reversible control of nanoscale volume structures may find multiple uses in applications requiring fluidic flow control, molecular separations, or nanoscale actuators.

METHODS AND MATERIALS

Planar Electrode Experiments. Planar electrodes were prepared on SiO_2-coated Si wafers (Silicon Quest International, Santa Clara, CA). Metal layers (50 Å Ti, 2000 Å Au) were patterned using photolithography and subsequently deposited using an electron beam evaporator. The wafers were cleaved into rectangular chips ~4 cm^2 in area. To provide electrical connectivity, a copper wire was affixed to the corner of each individual chip by silver-loaded epoxy (TRADUCT BA 2902, Tracon, Bedford, MA). The connection was then strengthened and insulated by coating with a nonconductive epoxy (FDA2T, Tracon, Bedford, MA). If a reduction in active electrode area was necessary to reduce current flow, the electrode was painted with fingernail polish. Polypyrrole films were deposited on the gold planar electrodes as previously described.[43–51] Pyrrole monomer solutions were prepared as solutions of 100 mM monomer (Acros Organics, Geel, Belgium) and 100 mM sodium dodecylbenzensulfonate (NaDBS) (Aldrich, St. Louis, MO) in H_2O. To synthesize the films, a constant voltage of 700 mV, *versus* an Ag/AgCl (3 M KCl) reference electrode and a platinum wire counter electrode, was applied for 30 s using an electrochemical workstation (model 660A CH Instruments electrochemical analyzer).

The pPy coatings were assessed by scraping an area of polymer from the center of the sample with forceps. This provided the abrupt change in height necessary for AFM measurements. Polypyrrole films were deposited to a 500 nm thickness, on the order of pPy films deposited on CNFs. Polypyrrole actuation experiments were observed in 100 mM NaDBS solution, using a Molecular Imaging PicoPlus AFM system operated in contact mode. Actuation data were obtained from longitudinal cross sections of continuous line scans. To accurately determine film characteristics from the resulting scans, data analysis software was written in The Mathworks Inc. Matlab 6.5.0. Swelling and shrinking of the pPy(DBS) films were controlled by applying −1.0 and 0.0 V *versus* a known reference using the electrochemical workstation.

Carbon Nanofiber—Polypyrrole Membrane Experiments. To fabricate polypyrrole−vertically aligned carbon nanofiber composites on silicon wafers, a 500 Å Ti layer was first deposited on the wafers with an electron beam evaporator for bulk electrical addressability. Then, nanofiber membranes were grown from photolithographically defined nickel catalyst stripes as previously described.[37,38] Briefly, catalyst stripes 2 μm wide, in the shape of squares with sides of 10, 25, 50, 100, and 150 μm, were patterned under a Karl Suss MA6 contact aligner. Then 30 nm of nickel catalyst was deposited with the electron beam evaporator and excess metal was lifted off in acetone. Individual wafers were placed in a dc-PECVD chamber. Wafers were heated to 600 °C and nanofiber synthesis was performed with 188 sccm NH_3 and 70 sccm C_2H_2 at 10 Torr and 1.0 A of plasma current. Carbon nanofibers grown under these conditions were found to be 8.5–9.5 μm tall with nominal diameters of 500 nm, measured at the base, and 300 nm, measured at the tip.

Wafers with the VACNF membrane structures were cleaved into rectangular chips ~6 cm^2 in area. A copper wire was affixed to the corner of each individual chip by silver-loaded epoxy and was further strengthened and insulated by coating with nonconductive epoxy (FDA2T, Tracon, Bedford, MA). The active electrode area was reduced by painting with fingernail polish. A rectangular-shaped area (~2 cm^2) immediately surrounding the VACNF membrane structures was left unpainted. The fingernail polish acted as an insulator to decrease the current flow from the bulk addressed electrode.

Polypyrrole films were then deposited on the VACNF membrane structures. Pyrrole monomer solutions were prepared as 100 mM monomer, 100 mM NaDBS in H_2O, and film synthesis was conducted at 700 mV for 30 s. The nominal thickness of the pPy films was found to be 150–200 nm, which reduced interfiber spacing from ~600–800 to ~250–350 nm. At longer depo-

sition times, the pPy coatings of adjacent nanofibers would grow together closing the "pores" in the membrane wall.

To provide fluidic access and to seal the top surface of the carbon nanofiber−polymer membrane structures, simple fluidic channels were fashioned from poly(dimethylsiloxane) (PDMS). Molds for channels 2 mm wide and 10 cm long were patterned on silicon wafers by contact photolithography. The areas of silicon not protected by photoresist were etched down 5.5 μm by inductively coupled SF_6-based plasma RIE. Prior to use, the silicon molds were primed with hexamethyldisiloxane priming agent to prevent PDMS from adhering during curing. PDMS was then poured over the silicon channel mold and cured at 60 °C for 90 min. Channels were cut from the mold with a scalpel to a channel length of ~1.5 mm, long enough to enclose approximately five to seven membrane structures.

Excess pPy was scraped from the titanium substrate with a scalpel leaving only a thin (~1 mm) strip of pPy surrounding the VACNF membrane structures. After the substrate was scraped, the PDMS channels and VACNF membrane structures were oxygen plasma cleaned and then immediately aligned and mated. Oxygen plasma cleaning promoted a stronger bond during mating. However, prolonged exposure of pPy-coated structures to oxygen plasma (<10 s, 100 W, 10 sccm O_2) appeared to be detrimental to polymer integrity. Because the PDMS channels were wide (2 mm) and were not supported by a rigid backing, sagging of PDMS into the channels was unavoidable. However, the PDMS would sufficiently separate from the substrate to allow flow of species upon wetting of the channel and actuation of the underlying pPy film.

For actuation experiments, the VACNF membrane structures were secured in a 100 × 15 mm style Petri dish by double-sided tape. A platinum wire, serving as a counter electrode, was fashioned into a U-shape and was wrapped around the VACNF membrane structures. The best results were attained when the counter wire was within 5 mm of the VACNFs, to better control the current during actuation. A chloride-coated silver wire was wrapped around the outer edge of the Petri dish and acted as a quasi-reference (+10 mV vs Ag/AgCl (3 M KCl) in 100 mM NaDBS).

To assess changes in membrane permeability during pPy actuation, fluorescently labeled species of varying sizes were used. Actuation experiments were observed using a Zeiss Axioscop 2FS epi-fluorescence microscope at 10× magnification. In a typical experiment, the fluorescently labeled species (*e.g.*, latex beads, Polysciences Inc., Warrington, PA) were suspended in 100 mM NaDBS. The Petri dish was filled with the solution until the fluidic channels were wetted. Fluorescent species would rapidly diffuse, completely wetting the ~1.5 mm length of microfluidic channel in ~10 s. Voltage was then potentiostatically applied, and fluorophore transport through the membrane structures was observed.

Acknowledgment. This research was supported by NIH Grant EB000657. A portion of this research was conducted at the Center for Nanophase Materials Sciences, which is sponsored at Oak Ridge National Laboratory by the Division of Scientific User Facilities, U.S. Department of Energy. A.V.M. and M.L.S. acknowledge support from the Materials Sciences and Engineering Division Program of the DOE Office of Science. This work was performed at the Oak Ridge National Laboratory, managed by UT-Battelle, LLC, for the U.S. DOE under Contract No. DE-AC05-00OR22725.

REFERENCES AND NOTES

1. Henry, J. D.; Lawler, L. F.; Kuo, C. H. A. Solid-Liquid Separation Process Based on Cross Flow and Electrofiltration. *AIChE J.* **1977**, *23*, 851–859.
2. Hernandez, A.; Martinez-Villa, F.; Ibanez, J. A.; Arribas, J. I.; Tejerina, A. F. An Experimentally Fitted and Simple Model for the Pores in Nucleopore Membranes. *Sep. Sci. Technol.* **1986**, *21*, 665–677.
3. Nystrom, M.; Lindstrom, M.; Matthiasson, E. Streaming Potential as a Tool in the Characterization of Ultrafiltration Membranes. *Colloids Surf.* **1989**, *36*, 297–312.
4. Sugawara, M.; Kojima, K.; Sazawa, H.; Umezawa, Y. Ion Channel Sensors. *Anal. Chem.* **1987**, *59*, 2842–2846.
5. Ballarin, B.; Brumlik, C. J.; Lawson, D. R.; Liang, W. B.; Vandyke, L. S.; Martin, C. R. Chemical Sensors Based on Ultrathin Film Composite Membranes - a New Concept in Sensor Design. *Anal. Chem.* **1992**, *64*, 2647–2651.
6. Kobayashi, Y.; Martin, C. R. Highly Sensitive Methods for Electroanalytical Chemistry Based on Nanotubule Membranes. *Anal. Chem.* **1999**, *71*, 3665–3672.
7. Wu, Z. Y.; Tang, J. L.; Cheng, Z. L.; Yang, X. R.; Wang, E. K. Ion Channel Behavior of Supported Bilayer Lipid Membranes on a Glassy Carbon Electrode. *Anal. Chem.* **2000**, *72*, 6030–6033.
8. Schwendeman, S. P.; Amidon, G. L.; Meyerhoff, M. E.; Levy, R. J. Modulated Drug Release Using Iontophoresis through Heterogeneous Cation Exchange Membranes-Membrane Preparation and Influence of Resin Cross-Linkage. *Macromolecules* **1992**, *25*, 2531–2540.
9. Keister, J. C.; Kasting, G. B. A Kinetic Model for Ion Transport across Skin. *J. Membr. Sci.* **1992**, *71*, 257–271.
10. Nolan, L. M. A.; Corish, J.; Corrigan, O. I. Electrical Properties of Human Stratum Corneum and Transdermal Drug Transport. *J. Chem. Soc., Faraday Trans.* **1993**, *89*, 2839–2845.
11. Lokuge, I.; Wang, X.; Bohn, P. W. Temperature-Controlled Flow Switching in Nanocapillary Array Membranes Mediated by Poly(N-isopropylacrylamide) Polymer Brushes Grafted by Atom Transfer Radical Polymerization. *Langmuir* **2007**, *23*, 305–311.
12. Song, L. Z.; Hobaugh, M. R.; Shustak, C.; Cheley, S.; Bayley, H.; Gouaux, J. E. Structure of Staphylococcal Alpha-Hemolysin, a Heptameric Transmembrane Pore. *Science* **1996**, *274*, 1859–1866.
13. Kasianowicz, J. J.; Brandin, E.; Branton, D.; Deamer, D. W. Characterization of Individual Polynucleotide Molecules Using a Membrane Channel. *Proc. Natl. Acad. Sci. U.S.A.* **1996**, *93*, 13770–13773.
14. Meller, A.; Nivon, L.; Branton, D. Voltage-Driven DNA Translocations through a Nanopore. *Phys. Rev. Lett.* **2001**, *86*, 3435–3438.
15. Hector, R. S.; Gin, M. S. Signal-Triggered Transmembrane Ion Transport Through Synthetic Channels. *Supramol. Chem.* **2005**, *17*, 129–134.
16. Kocer, A.; Walko, M.; Meijberg, W.; Feringa, B. L. A Light-Actuated Nanovalve Derived from a Channel Protein. *Science* **2005**, *309*, 755–758.
17. Dalvie, S. K.; Baltus, R. E. Transport Studies with Porous Alumina Membranes. *J. Membr. Sci.* **1992**, *71*, 247–255.
18. Kemery, P. J.; Steehler, J. K.; Bohn, P. W. Electric Field Mediated Transport in Nanometer Diameter Channels. *Langmuir* **1998**, *14*, 2884–2889.
19. Kuo, T. C.; Cannon, D. M.; Chen, Y. N.; Tulock, J. J.; Shannon, M. A.; Sweedler, J. V.; Bohn, P. W. Gateable Nanofluidic Interconnects for Multilayered Microfluidic Separation Systems. *Anal. Chem.* **2003**, *75*, 1861–1867.
20. Martin, C. R. Nanomaterials-a Membrane-Based Synthetic Approach. *Science* **1994**, *266*, 1961–1966.
21. Martin, C. R. Membrane-Based Synthesis of Nanomaterials. *Chem. Mater.* **1996**, *8*, 1739–1746.
22. Jirage, K. B.; Hulteen, J. C.; Martin, C. R. Nanotubule-Based Molecular Filtration Membranes. *Science* **1997**, *278*, 655–658.
23. Siwy, Z. S.; Gu, Y. C.; Spohr, H. A.; Baur, D.; Wolf-Reber, A.; Spohr, R.; Apel, P.; Korchev, Y. E. Nanofabricated Voltage-Gated Pore. *Biophys. J.* **2002**, *82*, 266A.
24. Sun, L.; Crooks, R. M. Single Carbon Nanotube Membranes: a Well-Defined Model for Studying Mass Transport through Nanoporous Materials. *J. Am. Chem. Soc.* **2000**, *122*, 12340–12345.
25. Miller, S. A.; Young, V. Y.; Martin, C. R. Electroosmotic Flow in Template-Prepared Carbon Nanotube Membranes. *J. Am. Chem. Soc.* **2001**, *123*, 12335–12342.
26. Li, J.; Stein, D.; McMullan, C.; Branton, D.; Aziz, M. J.; Golovchenko, J. A. Ion-Beam Sculpting at Nanometre Length Scales. *Nature* **2001**, *412*, 166–169.

27. Storm, A. J.; Chen, J. H.; Ling, X. S.; Zandbergen, H. W.; Dekker, C. Fabrication of Solid-State Nanopores with Single-Nanometre Precision. *Nat. Mater.* **2003**, 537–540.
28. Saleh, O. A.; Sohn, L. L. An Artificial Nanopore for Molecular Sensing. *Nano Lett.* **2003**, *3*, 37–38.
29. Huang, L. R.; Cox, E. C.; Austin, R. H.; Sturm, J. C. Continuous Particle Separation through Deterministic Lateral Displacement. *Science* **2004**, *304*, 987–990.
30. van Oudenaarden, A.; Boxer, S. G. Brownian Ratchets: Molecular Separations in Lipid Bilayers Supported on Patterned Arrays. *Science* **1999**, *285*, 1046–1048.
31. Chou, C. F.; Bakajin, O.; Turner, S. W. P.; Duke, T. A. J.; Chan, S. S.; Cox, E. C.; Craighead, H. G.; Austin, R. H. Sorting by Diffusion: An Asymmetric Obstacle Course for Continuous Molecular Separation. *Proc. Natl. Acad. Sci. U.S.A.* **1999**, *96*, 13762–13765.
32. Zhang, L.; Melechko, A. V.; Merkulov, V. I.; Guillorn, M. A.; Simpson, M. L.; Lowndes, D. H.; Doktycz, M. J. Controlled Transport of Latex Beads through Vertically Aligned Carbon Nanofiber Membranes. *Appl. Phys. Lett.* **2002**, *81*, 135–137.
33. Fletcher, B. L.; Hullander, E. D.; Melechko, A. V.; McKnight, T. E.; Klein, K. L.; Hensley, D. K.; Morrell, J. L.; Simpson, M. L.; Doktycz, M. J. Microarrays of Biomimetic Cells Formed by the Controlled Synthesis of Carbon Nanofiber Membranes. *Nano Lett.* **2004**, *4*, 1809–1814.
34. Fowlkes, J. D.; Fletcher, B. L.; Hullander, E. D.; Klein, K. L.; Hensley, D. K.; Melechko, A. V.; Simpson, M. L.; Doktycz, M. J. Tailored Transport through Vertically Aligned Carbon Nanofibre Membranes; Controlled Synthesis, Modelling, and Passive Diffusion Experiments. *Nanotechnology* **2005**, *16*, 3101–3109.
35. Fowlkes, J. D.; Hullander, E. D.; Fletcher, B. L.; Retterer, S. T.; Melechko, A. V.; Hensley, D. K.; Simpson, M. L.; Doktycz, M. J. Molecular Transport in a Crowded Volume Created from Vertically Aligned Carbon Nanofibres: A Fluorescence Recovery after Photobleaching Study. *Nanotechnology* **2006**, *17*, 5659–5668.
36. Merkulov, V. I.; Melechko, A. V.; Guillorn, M. A.; Simpson, M. L.; Lowndes, D. H.; Whealton, J. H.; Raridon, R. J. Controlled Alignment of Carbon Nanofibers in a Large-Scale Synthesis Process. *Appl. Phys. Lett.* **2002**, *80*, 4816–4818.
37. Merkulov, V. I.; Lowndes, D. H.; Wei, Y. Y.; Eres, G.; Voelkl, E. Patterned Growth of Individual and Multiple Vertically Aligned Carbon Nanofibers. *Appl. Phys. Lett.* **2000**, *76*, 3555–3557.
38. Ren, Z. F.; Huang, Z. P.; Wang, D. Z.; Wen, J. G.; Xu, J. W.; Wang, J. H.; Calvet, L. E.; Chen, J.; Klemic, J. F.; Reed, M. A. Growth of a Single Freestanding Multiwall Carbon Nanotube on Each Nanonickel Dot. *Appl. Phys. Lett.* **1999**, *75*, 1086–1088.
39. Chen, J. H.; Huang, Z. P.; Wang, D. Z.; Yang, S. X.; Wen, J. G.; Ren, Z. F. Electrochemical Synthesis of Polypyrrole/Carbon Nanotube Nanoscale Composites Using Well-Aligned Carbon Nanotube Arrays. *Appl. Phys. A* **2001**, *73*, 129–131.
40. Nguyen-Vu, T. D. B.; Chen, H.; Cassell, A. M.; Andrews, R.; Meyyappan, M.; Li, J. Vertically Aligned Carbon Nanofiber Arrays: An Advance Toward Electrical-Neural Interfaces. *Small* **2006**, *2*, 89–94.
41. Fletcher, B. L.; McKnight, T. E.; Fowlkes, J. D.; Allison, D. P.; Simpson, M. L.; Doktycz, M. J. Controlling the Dimensions of Carbon Nanofiber Structures through the Electropolymerization of Pyrrole. *Synth. Met.* **2007**, *157*, 282–289.
42. Guillorn, M. A.; McKnight, T. E.; Melechko, A. V.; Merkulov, V. I.; Britt, P. F.; Austin, D. W.; Lowndes, D. H.; Simpson, M. L. Individually Addressable Vertically Aligned Carbon Nanofiber-Based Electrochemical Probes. *J. Appl. Phys.* **2002**, *91*, 3824–3828.
43. Diaz, A. F.; Kanazawa, K. K.; Gardini, G. P. Electrochemical Polymerization of Pyrrole. *J. Chem. Soc., Chem. Commun.* **1979**, *14*, 635–636.
44. Smela, E. Microfabrication of PPy Microactuators and Other Conjugated Polymer Devices. *J. Micromech. Microeng.* **1999**, *9*, 1–18.
45. Bilger, R.; Heinze, J. Application of Electrochemical Quartz Microbalance To Determine the Stoichiometry of Ion Movement during Doping-Undoping Processes in Polypyrrole. *Synth. Met.* **1991**, *43*, 2893–2896.
46. Pei, Q. B.; Inganas, O. Electrochemical Applications of the Bending Beam Method. *J. Phys. Chem.* **1993**, *97*, 6034–6041.
47. Gandhi, M. R.; Murray, P.; Spinks, G. M.; Wallace, G. G. Mechanism of Electromechanical Actuation in Polypyrrole. *Synth. Met.* **1995**, *73*, 247–256.
48. Matencio, T.; De Paoli, M. A.; Peres, R. C. D.; Torresi, R. M.; Cordoba de Torresi, S. I. Ionic Exchanges in Dodecylbenzenesulfonate Doped Polypyrrole, Part I. Optical Beam Deflection Studies. *Synth. Met.* **1995**, *72*, 59–64.
49. Torresi, R. M.; Cordoba de Torresi, S. I.; Matencio, T.; De Paoli, M. A. Ionic Exchanges in Dodecylbenzenesulfonate Doped Polypyrrole, Part II. Electrochemical Quartz Crystal Microbalance Study. *Synth. Met.* **1995**, *72*, 283–287.
50. Smela, E.; Gadegaard, N. Surprising Volume Change in PPy(DBS): an Atomic Force Microscopy Study. *Adv. Mater.* **1999**, *11*, 953–957.
51. Smela, E.; Gadegaard, N. Volume Change in Polypyrrole Studied by Atomic Force Microscopy. *J. Phys. Chem. B* **2001**, *105*, 9395–9405.
52. Duffy, D. C.; McDonald, J. C.; Schueller, O. J. A.; Whitesides, G. M. Rapid Prototyping of Microfluidic Systems in Poly(dimethylsiloxane). *Anal. Chem.* **1998**, *70*, 4974–4984.